RESEARCH ARTICLE

ADVANCED
PHOTONICS
RESEARCH
Open Access

www.adpr-journal.com

Optically Pumped Terahertz Molecular Laser: Gain Factor and Validation up to 5.5 THz

Marie-Hélène Mammez,* Zachary Buchanan, Olivier Pirali, Marie-Aline Martin-Drumel, Joan Turut, Guillaume Ducournau, Sophie Eliet, Francis Hindle, Stefano Barbieri, Pascale Roy, Gaël Mouret, and Jean-François Lampin*

Quantum cascade laser-pumped terahertz (THz) gas lasers are at the edge of revolutionizing THz science where powerful yet tunable sources have long been lacking. Maybe one of the last remaining drawbacks to a wider use of these instruments lies in the lack of available databases of potentially lasing transitions for users. A new figure of merit, the molecular gain factor is proposed, that allows to discriminate transitions by their lasing potential. Using this factor, catalogs of THz laser lines of ammonia, both $^{14}NH_3$ and $^{15}NH_3$, up to 10 THz are reported. Demonstration of the use of these two catalogs, and of the pertinence of the molecular gain factor, is made by experimentally observing 32 laser lines of $^{14}NH_3$ and 5 lines of $^{15}NH_3$ up to 5.5 THz. Prospects to generalize the use of this molecular gain factor to a wide range of molecules are discussed.

M.-H. Mammez, F. Hindle, G. Mouret
Laboratoire de Physico-Chimie de l'Atmosphère (LPCA)
Université du Littoral Côte d'Opale
Avenue Schumann, F-59140 Dunkerque, France
E-mail: mmammez@univ-littoral.fr

Z. Buchanan
Department of Chemistry
University of California, Davis
One Shields Avenue, Davis, CA 95616, USA

Z. Buchanan, O. Pirali, M.-A. Martin-Drumel
Université Paris-Saclay
CNRS
Institut des Sciences Moléculaires d'Orsay
91405 Orsay, France

O. Pirali, P. Roy
SOLEIL Synchrotron
AILES Beamline
l'Orme des Merisiers
Saint-Aubin, F-91190 Gif-sur-Yvette, France

J. Turut, G. Ducournau, S. Eliet, S. Barbieri, J.-F. Lampin
Institut d'Electronique Microélectronique et Nanotechnologie (IEMN)
CNRS UMR 8520
Université de Lille
Avenue Poincaré, F-59652 Villeneuve d'Ascq Cedex, France
E-mail: jean-francois.lampin@univ-lille.fr

1. Introduction

Owing to significant technological progress in photonics and electronics, a wide range of terahertz (THz) applications, in particular ultrahigh-resolution gas-phase molecular spectroscopy, are now more than ever within reach.[1] Using solid-state technologies, THz frequencies can be obtained with photonic approaches by nonlinear effects—e.g., different frequency generation in crystals,[2] photomixing in photodetectors,[3] plasma generation[4]—or by direct generation—e.g., quantum cascade lasers (QCLs),[5–7] p-Ge lasers.[8] From the electronic side, microwave harmonic generation (Schottky diodes multiplication chains) can produce frequencies up to about 3 THz.[1,9,10] Alternatively, the great potential of gas lasers has been emphasized since their very first demonstration,[11] though it has been hindered by the long-standing difficulty to generate more than a handful of discrete frequencies. In the earliest designs, population inversion, or pumping, was obtained by exploiting the non-equilibrium thermodynamic properties of plasma discharges, an approach restricted to a very limited number of transitions of a few molecules.[12] Soon after, optically pumped far-infrared (FIR) molecular lasers were reported,[13] exploiting a CO_2 discharge laser as a powerful infrared (IR) pump source. Using this approach, a broader variety of molecules became available as gain medium, through selective pumping, although a major challenge remained to find coincidences between the discrete emission frequencies of the IR pump and the absorption transitions of the active molecule. An imperfect resonance reduces drastically the gain and then requires a very powerful pump laser to reach the lasing threshold.[14] THz spectrometers that use such molecular lasers pumped by CO_2 lasers are usually very bulky, energy intensive, and require both a lot of different molecules to cover the THz range and a strong expertise.[1,15–19]

Because of their continuous tunability, solid-state pump sources overcome the aforementioned difficulty to generate the adequate frequency for a molecular gain medium. Pulsed optical parametric oscillators (OPOs) have proven efficient pump sources to generate mid-infrared (MIR) beams[20]—initiating the rise of "gas photonics"[21]—while MIR continuous-wave (CW) QCLs[22] have enabled the demonstration of the first THz molecular laser optically pumped by a solid-state laser.[23] Even though the latter breakthrough is only in its early stages

of development,[24–27] it appears to have the capacity to generate a virtually endless number of THz laser frequencies by exploiting a large range of molecular gases as the gain medium. This property makes this THz molecular laser a promising local oscillator for heterodyne experiments, provided that reliable laser linelists exist.[28] Available catalogs of pump and laser pairs of frequencies have traditionally been built empirically using time-consuming procedures[29] and the number of lines remains far from exhaustive. Nowadays, molecular databases, developed for atmospheric and astrophysical applications, are complete enough to enable a systematic prediction of accurate pump and laser frequencies.

Among the possible gain media, ammonia (NH_3), as a high gain molecule with many possible emission frequencies, has focused particular interest.[23,24,27] Only a handful of laser transitions have been generated in NH_3, mainly in the 1970s and 1980s (see Tables S1 and S2, Supporting Information),[27,30–35] due to a limited number of coincidences between the pump frequencies emitted by the CO_2 and N_2O lasers and the MIR absorption spectrum of NH_3. Nevertheless, NH_3 is ideally suited for the generation of optically pumped THz laser lines because of 1) its large permanent dipole moment of about 1.5D; 2) its strong vibrational transition dipole moments (e.g., 0.2D for the sQ(3,3) transition of the fundamental ν_2 band[26]); and 3) its "umbrella" inversion, allowed by tunnelling effect, resulting in a splitting of rotational levels (a property that has enabled the observation of the first maser effect[36]), yielding a number of THz transitions between the tunnelling states. Using $^{14}NH_3$ as gain medium, the highest CW conversion efficiency in the THz has recently been obtained.[26] It is also worth mentioning that NH_3 possesses about 9 bars of vapor pressure at room temperature, making it relatively convenient to handle. Finally, NH_3 is a well-known prototype molecule from a molecular physics point of view: its spectroscopic characterisation has been very well documented, another advantage of using this molecule to build the new generation of THz molecular lasers.

As THz molecular lasers pumped by a QCL will potentially generate a huge quantity of new THz frequencies, a method that would allow comparison and classification of laser lines by their lasing potential is more than ever needed. The aims of the present paper are threefold: 1) define a purely molecular-based figure of merit (i.e., excluding experimental and technical parameters proper to each laser design), hereafter called the molecular gain factor G_m, that allows identification of the MIR/THz transitions pairs exhibiting the strongest lasing potential; 2) provide a list of possible THz laser lines that can be obtained using a MIR pump laser in the 10 μm range and ammonia as gain medium (both $^{14}NH_3$ and $^{15}NH_3$); 3) verify experimentally the validity of both our figure of merit and catalogs by detecting various laser lines up to 5.5 THz. In the following, after defining the molecular gain factor, we report two laser catalogs, for $^{14}NH_3$ and $^{15}NH_3$, that have been built using available spectroscopic information on the HITRAN database.[37] In the catalogs, each entry contains the MIR pump and THz laser frequencies—and associated quantum numbers (QN) involved in the transitions—and the associated molecular gain factor. Using these catalogs, we were able to measure 32 laser lines of $^{14}NH_3$ and 5 of $^{15}NH_3$, up to 5.5 THz, using a new prototype of NH_3 laser (described in Section 4.4). This represents a significant extension of the observed laser lines of both molecules in CW regime, previously limited to 5 and 12 lines for $^{14}NH_3$ and $^{15}NH_3$, respectively (see Tables S1 and S2, Supporting Information). In the Results section, we provide an extract of the catalogs (the full catalogs from 100 GHz to 10 THz are given in the Supporting Information) together with our measurements. Perspectives of the present work concerning the laser catalogs and the THz molecular laser are discussed.

2. Results

2.1. Molecular Gain Factor

To establish the potential for a pair of pump/laser transitions having sufficient gain to overcome the losses of a resonant cavity, we introduce the molecular gain factor, G_m. For one molecule of gain medium and a given pair of pump/laser transitions, the small-signal gain coefficient is expressed as the product of two factors

$$\gamma_0 = G_m K \tag{1}$$

with

$$G_m = \frac{S'_{02} B_{21}}{\nu_{02}^2} \frac{Mc}{2\pi N_A k_B T} \tag{2}$$

and K a factor depending on the relaxation rate and pump laser performances (expressed in $J\,m^{-5}$). The three involved energy levels (0, 1, and 2) are ranked by increasing energy thus the pump transition occurs from the level 0 to the level 2 and the THz laser one from 2 to 1. S'_{02} is the line strength of the pump transition (in $m^2\,s^{-1}$) and ν_{02} its frequency (in Hz), B_{21} is the Einstein coefficient of stimulated emission for the THz transition (in $m^3\,J^{-1}\,s^{-2}$), M is the molar mass of the molecular gas (in $kg\,mol^{-1}$), and T is the temperature (in K). The constants c, N_A, and k_B are expressed in SI units. G_m is thus expressed in SI units of $m^4\,J^{-1}$. For the sake of simplicity, the uG_m notation will be used in the following when referring to G_m units. Details on the derivation of this molecular gain factor and its units can be found in Section 4.2.

Apart from the temperature, G_m relies only on molecular parameters and fundamental constants. If the technical parameters (e.g., pump power density, gain medium pressure, and molecular laser design) of the laser are kept constant, the higher the value of G_m, the lower the molecular laser threshold and thus the higher the THz output power. Consequently, G_m can be used to classify the multitude of possible laser transitions of a given molecule, here two isotopologues of ammonia, against their potential to produce an intense radiation. In addition, this factor can also be used to compare the lasing potential of different molecular species.

2.2. Catalogs of MIR-Pumped THz-Laser Transitions of Ammonia

The first step in establishing lists of possible laser lines is to identify all possible pairs of pump/laser transitions, i.e., transitions sharing a common level, as sketched in **Figure 1**. Two possible
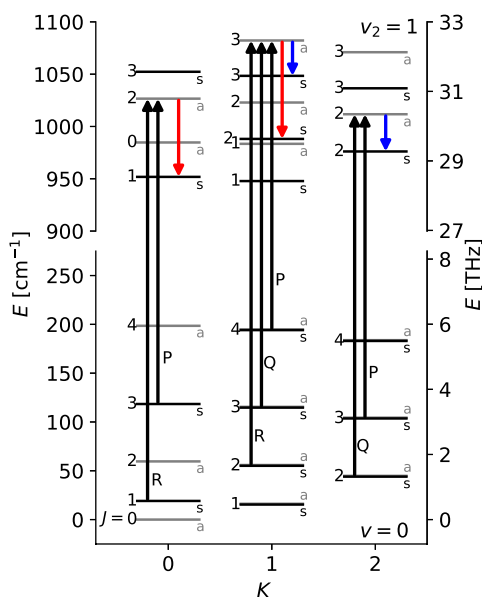
Figure 1. Schematic energy-level diagram of $^{14}NH_3$ in the ground and $\nu_2 = 1$ states for $K \leq 2$ and $J_{up} \leq 3$. Levels of "s" symmetry are plotted using dark lines, those of "a" symmetry using gray lines. Illustration of possible pump (black arrows)/laser (red and blue arrows) transitions. Rotation-inversion lines ($\Delta J = 1$) are represented in red, pure inversion ones ($\Delta J = 0$) in blue.

symmetric bending ν_2 of NH_3, between 560 and 1360 cm^{-1} for $^{14}NH_3$ and between 533 and 1295 cm^{-1} for $^{15}NH_3$, while the frequency range of the paired THz transition has been limited to the 0.1–10 THz (3.3–333 cm^{-1}) region. We have further restrained our investigations to the $\Delta K = 0$ transitions, presumably the strongest ones (see Section 4.1). Only the pairs of transitions exhibiting an exploitable molecular gain factor, i.e., within five orders of magnitude of the strongest one (here $G_m > 1 \times 10^{-21} \, uG_m$) are reported. Under these restrictions, a total of 326 potential laser lines accessible via 808 pump/laser combinations for $^{14}NH_3$ (Table S3, Supporting Information) and 285 potential laser lines accessible via 733 pump/laser combinations for $^{15}NH_3$ (Table S4, Supporting Information) are reported in this work. Subsets of these tables, displaying only the THz laser lines with the strongest potential, their paired MIR pump frequency and molecular gain factor, are reported in **Table 1**.

It is important to note that the accuracy of the frequencies in the proposed lists and of the molecular gain factor values is intrinsically linked to that of the spectroscopic databases used to build the catalog (here HITRAN). Additional information on this particular point can be found in Section 4.3. In the tables reported in this article, frequencies are those from the HITRAN database;[37–41] experimental values can differ and for some transitions, frequencies found in the JPL database[42] can be more accurate.

In Tables S3 and S4, Supporting Information, each THz laser line is reported together with the possible MIR pump frequencies, the corresponding QN, the molecular gain factors, and the polarization of the THz radiation with respect to the pump polarization. Because of spectroscopic considerations (see Section 4.1), several combinations of pump/laser lines are generally possible. Each of the THz laser lines can theoretically be generated by one of three MIR pumping frequencies, corresponding to the possible absorptions in the P, Q, and R branches of the ν_2 band (Figure 1). Alternatively, it is possible that a pump

laser transitions are distinguishable: those sharing a common level in the excited state and those sharing a common level in the ground state (often called "refilling transition"[13,25]). The latter type of lasing, which has been found to be significantly less favorable than the former one due to high required pump power,[25] will not be further discussed here.

To establish our catalogs, we have restrained the spectral range of the pump transitions to the rovibrational transitions of the

Table 1. List of the ten $^{14}NH_3$ laser lines in the ν_2 band exhibiting the strongest gain factor in the 0.1–10 THz range. The star symbols indicate the experimentally observed lines.

$^{14}NH_3$					$^{15}NH_3$				
THz laser [GHz]	THz QN	MIR pump [cm^{-1}]	G_m [uG_m]		THz laser [GHz]	THz QN	MIR pump [cm^{-1}]	G_m [uG_m]	
1073.0499	sQ(3,3)	967.3463	1.3 E-17	★	1035.2013	sQ(3,3)	962.1285	1.5 E-17	★
1115.0810	sQ(6,6)	965.3539	1.2 E-17	★	1075.997	sQ(6,6)	960.143	1.3 E-17	a)
1082.5928	sQ(4,4)	966.8147	7.5 E-18	★	1044.4973	sQ(4,4)	961.6018	8.3 E-18	★
1096.5904	sQ(5,5)	966.1511	7.2 E-18	★	1058.0557	sQ(5,5)	960.9397	8.0 E-18	
769.7102	aR(2,0)	992.6987	5.2 E-18	★	802.9860	aR(2,0)	988.6486	5.7 E-18	
466.2458	sP(1,0)	948.2320	4.8 E-18		430.0409	sP(1,0)	943.0531	5.3 E-18	
1138.2110	sQ(7,7)	964.4240	4.7 E-18	★	1098.447	sQ(7,7)	959.213	5.0 E-18	a)
3373.6128	sR(3,0)	1046.4055	4.6 E-18	★	3332.3527	sR(3,0)	1041.0901	5.2 E-18	★
1067.6770	sQ(2,2)	967.7384	4.6 E-18	★	1030.1163	sQ(2,2)	962.5199	5.0 E-18	
2035.4532	aR(4,0)	1034.2448	4.6 E-18	★	2064.9399	aR(4,0)	1030.1412	4.9 E-18	★

a)These lines are absent from our catalogs because one of the two lines is not reported in the HITRAN database. The reported frequencies are taken from ref. [51]. For these transitions, the G_m factor of the corresponding pair of transitions in $^{14}NH_3$ was scaled by the ratio of molar masses between the two species.

ADVANCED
SCIENCE NEWS
www.advancedsciencenews.com

ADVANCED
PHOTONICS
RESEARCH
Open Access
www.adpr-journal.com

transition shares a common upper state with two THz transitions yielding to a competition between the two laser frequencies. For instance, upper states with $J > K$, $K \neq 0$, and "a" inversion symmetry can generate two laser frequencies by either pure inversion or rotation-inversion (Figure 1, central panel). Laser emission can either oscillate between the two possible frequencies or, because of gain values and/or laser cavity losses, possibly favor one of them. These transitions are labeled with an asterisk in Tables S3 and S4, Supporting Information, and listed in Tables S5 and S6, Supporting Information. One can also notice in Tables S3 and S4, Supporting Information, that, for several THz transitions, either the P, or Q, or R pumping branch is missing. This can be due to the restrictions applied to the building parameters of our database (G_m cut-off, MIR or THz frequency ranges) or to spectroscopic selection rules. As an example, for $J = K$ energy levels in $v_2 = 1$, pumping from the R branch is not allowed because of the $J \geqslant K$ requirement, and only a pure inversion laser transition is allowed (Figure 1). Another example is that of the $K = 0$ levels which can not be reached using Q-branch transitions and for which no laser pure inversion transition is allowed because of the a $\leftrightarrow$ s symmetry selection rule (Figure 1).

A graphical representation of the two catalogs is proposed in **Figure 2**. Individual plots for $^{14}NH_3$ and $^{15}NH_3$ are displayed in Figure S1, Supporting Information. On these figures, the possible pairs of IR pump frequencies and THz laser frequencies are plotted with their corresponding molecular gain factors. Such graphical representation of laser frequencies highlights the broadband coverage accessible using NH_3 as gain medium over the entire THz region. Every colored circle corresponds to a potential laser line generated by MIR pumping in the v_2 band which exhibits a molecular gain factor higher than the chosen cut-off ($G_m > 1 \times 10^{-21}$ uG_m). The figure reveals a structured distribution of THz frequencies relative to the MIR frequencies resulting from the spectroscopic properties of the molecules. Regions of P-, Q-, and R-branches pump transitions on one hand, and of pure inversion and rotation-inversion laser transitions, on the other hand, are clearly distinguishable (see Figure S1 for a graphical representation of the corresponding areas). This figure also reveals a high density group of high G_m laser lines (larger than 1×10^{-18} uG_m) accessible around 1 THz thanks to the unique properties of the pure inversion transitions within
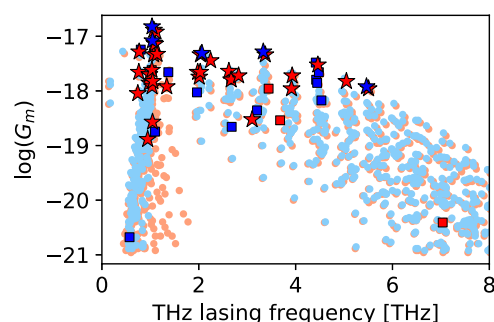

Figure 3. Molecular gain factor as a function of the THz laser frequencies of $^{14}NH_3$ (in light red) and $^{15}NH_3$ (in light blue). The observed laser transitions in this work, covering two orders of magnitudes of G_m values, are highlighted by a star symbol (of the respective darker color). Laser transitions previously reported for both species are indicated by squares (using the same color coding).

$v_2 = 1$ of NH_3. A zoom displayed on the right panels of Figure 2 and S1, Supporting Information, shows the J and K distribution in this region.

A second graphical representation, where the G_m of both $^{14}NH_3$ and $^{15}NH_3$ is plotted as a function of the THz laser frequency, is presented in **Figure 3** (corresponding individual plots are reported in Figure S2, Supporting Information). The change between $^{14}NH_3$ and $^{15}NH_3$ isotopologue results in THz frequency shifts of a few tens of GHz (typically 30–40 GHz) with similar G_m values. One can notice the absence of some THz lines of $^{15}NH_3$, particularly in the 1–2 THz range, as a result of missing transitions from the HITRAN database.

2.3. Validation of the Figure of Merit and Catalogs

Using the newly established catalogs to guide searches for laser transitions of ammonia using our QCL-pumped laser set-up, 32 pairs of MIR pump/THz laser lines for $^{14}NH_3$ and 5 laser lines for $^{15}NH_3$ were generated in the range 0.74–5.5 THz. Of these, 30 laser frequencies for $^{14}NH_3$ and all frequencies for $^{15}NH_3$ are reported for the first time in a resonant pumping CW regime.
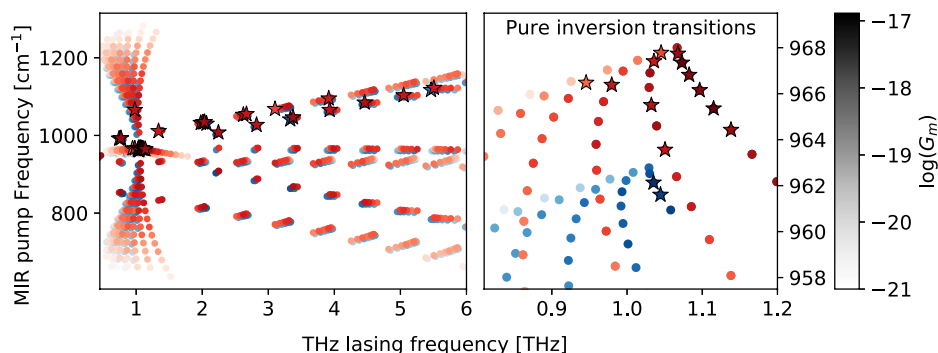

Figure 2. Lasing THz transitions of $^{14}NH_3$ (in shades of red) and $^{15}NH_3$ (in shades of blue), and corresponding molecular gain factors as a function of the MIR pump frequency. Predicted and observed lasing lines are represented by dot and star symbols, respectively. Left panel: IR probes in the 600–1300 cm^{-1} region and THz laser lines below 6 THz. Right panel: Zoom onto the pure inversion transitions accessible by Q-branch pumping. The color coding ranges from light-to-dark color with increasing G_m values, in logarithmic scale.

Our QCL pump laser limits the pumping range to 920–1330 cm^{-1}, corresponding to Q- and R-branch MIR pumping of the ν_2 band of both $^{14}NH_3$ and $^{15}NH_3$ isotopologues used as gain media. The highest THz frequency is limited by the molecular laser setup, in particular the material of the output window (see Section 4.4). Tables 2 and 3 summarize the laser lines observed between

Table 2. Observed laser transitions of $^{14}NH_3$ in its $\nu_2 = 1$ vibrational state and associated MIR pump frequency and molecular gain factor. Lines having a possible competing laser line are labelled with an asterisk. For each observed laser line, the measured signal (S) is reported. Details about the experimental measurements can be found in the experimental section.

THz laser [GHz]	MIR pump [cm^{-1}]		G_m [uG_m]	S [mV]
Rotation-Inversion				
741.7881	991.6905		9.0 E-19	3.1
762.8525	992.4503		2.2 E-18	5.2
769.7102	992.6987		5.2 E-18	7.5
1338.6790	1011.2036		1.2 E-18	9.0
1978.1120	1032.1310		2.2 E-18	8.5
2010.3707	1033.3158		1.8 E-18	12.5
2029.2006	1034.0127		2.2 E-18	20.0
2035.4532	1034.2448		4.6 E-18	21.4
2244.4659	1007.5471		3.6 E-18	4.7
2622.0015	1053.1304		2.3 E-18	12.5
2669.4110	1054.9126		1.6 E-18	14.0
2822.2564	1027.0470		1.9 E-18	10.7
3101.5415	1067.9744		3.0 E-19	0.6
3373.6128	1046.4055		4.6 E-18	16.0
3915.0670	1095.1293		1.1 E-18	9.4
3928.6856	1065.5943		1.9 E-18	12.0
4458.8750	1084.6290		3.0 E-18	3.8
5048.5821	1103.4412		1.5 E-18	5.4
5505.9143	1122.1853		1.1 E-18	4.0
Pure Inversion				
945.6048	*	966.4736	1.3 E-19	0.3
979.6498	*a)	966.3799	1.4 E-18	6.4
979.6498	*a)	1065.5654	2.0 E-18	10.0
1032.3214	*	965.4994	2.4 E-18	7.7
1035.8161	*	967.4067	1.2 E-18	5.8
1045.3191	*	967.7747	2.7 E-19	1.7
1050.5203	*	963.5585	1.5 E-18	6.0
1067.6770		967.7384	4.6 E-18	5.8
1073.0499		967.3463	1.3 E-17	8.9
1082.5928		966.8147	7.5 E-18	9.3
1096.5904		966.1511	7.2 E-18	4.0
1115.0810		965.3539	1.2 E-17	11.6
1138.2110		964.4240	4.7 E-18	8.3

a)Example of a THz line accessible from two different MIR pump transition.

Table 3. Observed lasing transitions of $^{15}NH_3$ within the $\nu_2 = 1$ vibrational state and associated MIR pump frequency and molecular gain factor. None of them possesses a competing line. When available, the signal (S) measured is reported. Details about the experimental measurements can be found in the experimental section.

THz laser [GHz]	MIR pump [cm^{-1}]	G_m [uG_m]	S [mV]
Rotation-Inversion			
2064.9399	1030.1412	4.9 E-18	–
3332.3527	1041.0901	5.2 E-18	3.5
5463.2430	1116.9334	1.2 E-18	3.2
Pure Inversion			
1035.2013	962.1285	1.5 E-17	5.0
1044.4973	961.6018	8.3 E-18	7.4

740 GHz and 6 THz for $^{14}NH_3$ and $^{15}NH_3$, respectively. Among the 10 lines exhibiting the strongest molecular gain factors reported in Table 1, 9 lines of $^{14}NH_3$ (all of those accessible using our instrument) and 4 of $^{15}NH_3$ have been experimentally verified. Note that the generation of the remaining lines were not attempted but they are expected to be intense laser lines as well. These results demonstrate the reliability of the catalog to predict accurate frequencies and molecular gain factors for potential laser lines as well as the strength of the experimental set-up to generate a large number of THz laser lines.

One can notice in Table 2 that, among the 32 pairs of transitions, the same THz line at 979.6498 GHz can be obtained from two different MIR pump transitions: either from a Q-branch pumping at 966.3799 cm^{-1} or from a R-branch one at 1065.5654 cm^{-1}. The relative THz power measured for these two pumping schemes follows what expected from the calculated G_m values. When multiple pump transitions yield the same laser line, the choice of the MIR pump transition is guided by both the frequency range accessible by the pump laser and the G_m value of the pump/laser pair. Alternatively, competitions between laser lines involving the same upper level frequently occur. In the case of $^{14}NH_3$, the pump frequency at 1027.0470 cm^{-1} yields two possible laser transitions in the THz range accessible using our setup: 1014.0847 GHz or 2822.2564 GHz. The molecular gain factor of the line at 2822.2564 GHz is 4.4 times larger than that of the line at 1014.0847 GHz. Experimentally, we measured a single emission line at 2.8 THz, as expected from the G_m values. Nevertheless, the cavity losses can not be neglected for competing transitions. For example, a pump transition located at 966.4736 cm^{-1} leads to the detection of a laser line at 945.6048 GHz (with $G_m = 1.3 \times 10^{-19}$ uG_m), even if the molecular gain factor of the competing transition at 3950.7233 GHz is about three times larger, because the latter is less favorable in our laser setup (plausibly due to larger losses for the higher frequency).

Pure inversion transitions of $^{14}NH_3$ and $^{15}NH_3$ are all located around 1 THz and allow for a deep coverage of that spectral region (Figure 3). Alternatively, rotation-inversion transitions allow the generation of laser lines over the entire THz region. The remaining transitions observed here belong to this group
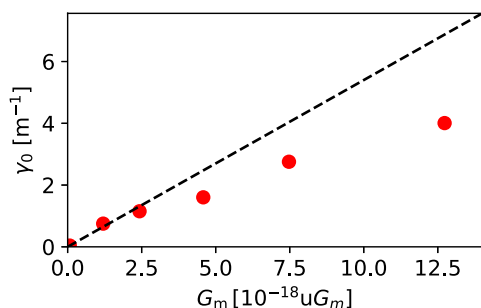
**ADVANCED
SCIENCE NEWS**

www.advancedsciencenews.com

**ADVANCED
PHOTONICS
RESEARCH**

www.adpr-journal.com

Figure 4. Measured unsaturated gains γ_0 as a function of the calculated molecular gain factor G_m for six pairs of pump/probe transitions (red dots, see Table S7, Supporting Information). The black dashed line represents the fit of the three first points for which the power density of the pump can be considered uniform (see text).

and span from 741.8 GHz to 5.5 THz. The strongest laser signal measured with our set-up was obtained using the aR(4,0) rotation-inversion transition of $^{14}NH_3$ located at 2.035 THz. A signal of 21.4 mV was measured for that line on the pyroelectric detector (Table 2) which corresponds to about 300 µW.

The G_m figure of merit is further validated by direct measurements of unsaturated gain values γ_0 for six pure inversion transitions of $^{14}NH_3$ (**Figure 4** and Table S7, Supporting Information, see Section 4.5 for details). One can notice the overall agreement between the gain measured and the calculated molecular gain factor G_m. By definition and assuming a uniform power density of the pump P_p, the gain is the product of G_m by a factor K, a parameter which depends on the relaxation rate Γ (see Section 4.2 for a detailed demonstration). In practice, P_p can only be approximated as spatially uniform for small line strengths of the pump transition (S'_{02}); for large S'_{02} values, an exponential decay of P_p along the gas cell is expected, although not taken into account in our G_m calculation. Consequently, a linear dependence of γ_0 with G_m can only be expected experimentally for small S'_{02} values, i.e., small G_m values. Indeed, deviation from linearity is observed on Figure 4 beyond the first three points and the experimental points with high G_m exhibit γ_0 values underestimated compared with the linear fit. From the linear regression presented on Figure 4 and considering a pressure of 2 Pa and a pump power density of $P_p = 255 \, W \, m^{-2}$ that were used for the measurements, a relaxation rate Γ of about $2.5 \times 10^5 \, s^{-1}$ can be estimated, a value in agreement with the $2.6 \times 10^5 \, s^{-1}$ value calculated in Section 4.5.

3. Conclusions

Among the suitable chemical species easily available in all laboratories, ammonia is an excellent candidate for the development of the next generation of optically pumped molecular lasers. It is obvious that such molecular lasers used as local oscillators (LO) can be valuable for a wide range of applications, starting with mixing of these new laser sources with THz radiations of different origins. Our group has already demonstrated the successful heterodyne mixing of a prototype of QCL-pumped molecular laser with synchrotron radiation around 1 THz[28] and the

present results allow us to envision new measurements at higher frequencies. Another potential application for radio-astronomy is worth mentioning. For instance, there is a near-coincidence between the aR(4,2) $^{14}NH_3$ laser line located at 2010.371 GHz with the $J = 1 - 0$ transition of HeH$^+$ cation at 2010.184 GHz, which was recently observed in a planetary nebula.[43] The frequency difference is sufficiently low to allow for heterodyne detection of this line using Schottky diodes or HEB as mixers. Other coincidences of this type exist and will certainly boost the future development of such LO to support new generation of THz observational platforms.

The relatively basic pump/laser process exploited in this paper can easily be generalized to the numerous molecules possessing relatively intense IR absorption bands and allowing pure rotation transitions in the THz range. In this context, we can foresee that the number of generated THz frequencies will increase by orders of magnitude by using various molecules and their isotopic variants. As shown in the present work, the simple extrapolation of $^{14}NH_3$ gain medium to the $^{15}NH_3$ isotopologue directly allows to double the number of laser lines, while using strictly identical experimental conditions. Obviously, with some instrumental effort, pump frequencies can be adjusted to different spectral regions in order to access other fundamental bands of various molecules, as well as overtones and combinations bands providing even more possibilities to generate THz lasers lines. Such opportunities require to sort out and organize molecules and their energy levels allowing the generation of THz laser processes. Our study demonstrates, using the NH_3 molecule, that the generation of such database is of great help to guide the experimental production of new laser lines. To increase the number of entries in our laser database, we set-up a very versatile code interrogating HITRAN molecular spectroscopy database in order to extract all necessary information (energy levels, intensities, and Einstein coefficients of MIR and THz transitions) to generate new THz lines for any molecules already reported in HITRAN. The description of the method used to generate the code is given in Section 4. However, such laser database relies entirely on the accuracy of the spectroscopic molecular characterization. Even though a few lines are currently missing for $^{15}NH_3$, our work reveals that the HITRAN database, which is constantly improving, is well suited to predict the position and strength of ammonia laser lines.

Finally, deuterated isotopologues of ammonia are other good candidates for generating new THz laser lines. In particular, as for the H isotopologues, the rotational transitions will allow access to numerous frequencies higher than 1 THz.[44,45] Establishing their THz line catalogs, however, requires an investment from the spectroscopy community to record and analyze their FIR spectra in order to update the spectroscopic databases.

4. Experimental Section

4.1. General Considerations

The principle of MIR-pumped THz lasers is based on a population inversion achieved by pumping population, using a ro-vibrational transition, from a state populated at room temperature to one that is not. In the following, we will restrain our study to the

ground and $\nu_2 = 1$ states of $^{14}NH_3$ and $^{15}NH_3$, although the general equations we report can be transferred to virtually any molecule and vibrational state if the hypotheses are fulfilled.

In our case, the THz laser is pumped by a MIR laser in the 10 μm range, therefore accurate values for the energy levels involving two vibrational states, namely the ground state (GS) and $\nu_2 = 1$ (around 950 cm^{-1} for both $^{14}NH_3$ and $^{15}NH_3$), are required. As a symmetric top species, the rotational structure of NH$_3$ is described using J (the total rotation angular momentum) and K (the projection of J on the C$_3$ symmetry axis) quantum numbers. In addition to the conventional energy-level diagram for symmetric tops, NH$_3$ is subject to the well-known tunnelling motion of the N nucleus through the plane formed by the 3 H atoms. This tunnelling effect splits each rotational level with $K \neq 0$ into two components, one symmetric (s) and one antisymmetric (a).

Rotational transitions within a nondegenerate vibrational state (the THz emission in our case) are categorized as pure inversion or rotation-inversion following the respective selection rules:

$$\Delta J = 0; \quad \Delta K = 0; \quad a \rightarrow s; \tag{3}$$

$$\Delta J = \pm 1; \quad \Delta K = 0; \quad a \rightarrow s; \quad s \rightarrow a \tag{4}$$

By convention, the inversion symmetry located to the left of the arrow corresponds to the higher energy level. For a given J, the "a" level lies at higher energy than the "s" one (e.g., see Figure 1).

Selection rules for the ro-vibration transitions within the $\nu_2 = 1 \leftarrow$ GS (IR absorption) are:

$$\Delta J = 0, \pm 1; \quad \Delta K = 0; \quad a \leftarrow s; \quad s \leftarrow a \tag{5}$$

It is worth noting that "forbidden" $\Delta K = 3$ transitions exist and exhibit intensities about two orders of magnitude lower than the corresponding $\Delta K = 0$ transition.[46] These transitions are beyond the scope of this article, in part because in their current state, databases do not allow to reproduce them satisfactorily,[46] and because the expected G_m values should be rather small. A schematic representation of the energy-level diagram of the lowest rotational states of NH$_3$ is displayed in Figure 1 for the ground and $\nu_2 = 1$ states, the latter containing less than 1% of the ground state population at room temperature. Examples of rotation-inversion ($\Delta J \neq 0$, left panel), pure inversion ($\Delta J = 0$, right panel), and an example of competition between THz laser lines from a single upper level (middle panel) are given on Figure 1. For simplicity, the quantum numbers associated with each transition are usually given in the absorption convention a/s$_{low}$P/Q/R(J_{low}, K_{low}) with P, Q, R corresponding to $\Delta J = J_{up} - J_{low} = -1, 0, +1$, respectively, and "up" and "low" to the upper and lower levels involved in the transition.

The large intensities of MIR and THz transitions of NH$_3$, owing to the large ν_2 transition moment and permanent dipole moment, respectively, are necessary to obtain high gain values of the laser. In the MIR, intense rotation-vibration transitions ensure an efficient population transfer from the GS to $\nu_2 = 1$. This is reinforced by the fact that NH$_3$ being a light molecule, the moments of inertia are relatively small leading to a relatively

limited numbers of rotational levels populated at room temperature in the ground vibrational state, and hence a significant population within each of these levels. In addition, the pure inversion and rotation-inversion transitions occurring within the excited states are intense, allowing laser effects at low threshold.

4.2. Derivation of the Molecular Gain Factor of a Pair of Pump/Laser Transitions

To initiate a laser process, the small-signal gain, or unsaturated gain, must exceed the total losses.[47] This parameter is critical to realise a laser regardless of any consideration of the characteristics of the cavity. We derive here the small-signal gain of an optically pumped molecular gas far from saturation, at low pressure in the Doppler regime, and under thermal equilibrium prior to pumping.

We consider a three energy levels scheme with the levels labelled 0, 1, and 2 ($E_0 < E_1 < E_2$). The MIR pumping transition occurs between levels 0 and 2, with $E_2 - E_0 = h\nu_{02}$, and the THz laser one between levels 2 and 1, at energy $E_2 - E_1 = h\nu_{21}$, where the energies are expressed in J, h is the Planck constant in J s, c is the speed of light in m s^{-1}, and ν are the frequencies of the transitions expressed in Hz (or s^{-1}). SI units will be used throughout the following demonstration. At room temperature and under thermal equilibrium, the populations in levels 1 and 2 can be considered null ($N_1 = N_2 = 0$) prior to pumping if the energy of these levels is high compared to k_BT, which is the case for the rotational levels that can be accessed using a 10 μm ($\approx 5 k_BT$) QCL pump laser. The optical MIR pumping from level 0 to 2 thus yields an inversion of population between the levels 2 and 1, and the THz photons flux is amplified by stimulated emission.

The laser gain along a distance d of gain medium at a frequency ν is given by:

$$G(\nu) = \frac{I}{I_0} = \exp(\alpha_{21}(\nu)d) > 1 \tag{6}$$

where I_0 and I are the optical intensity, before and after crossing the gain medium (in W m^{-2}), respectively, and $\alpha_{21}(\nu)$ is the gain coefficient (in m^{-1}). In the case of a small-signal gain or unsaturated gain regime, the gain coefficient α_{21} can be approximated as $\alpha_{21}(\nu) = \gamma_0(\nu)$.

The small-signal gain coefficient is expressed as:[47]

$$\gamma_0(\nu) = \sigma_{21}(N_2 - N_1) = (N_2 - N_1)\frac{h\nu B_{21}}{c}g(\nu) \tag{7}$$

where σ_{21} is the stimulated emission cross section of the THz transition (in m^2), B_{21} is the Einstein coefficient for the stimulated emission of the THz transition (in m^3 J^{-1} s^{-2}), and $g(\nu)$ is the lineshape function (in s). The populations N_2 and N_1 are expressed in m^{-3}.

At the center of the laser transition, under thermal equilibrium assumption ($N_1 = 0$), and assuming a Doppler linewidth, Equation (7) becomes:

$$\gamma_0(\nu_{21}) = N_2 h B_{21} \sqrt{\frac{M}{2\pi N_A k_B T}} \tag{8}$$

where M is the molar mass of the molecular gas (in $kg\,mol^{-1}$), N_A is the Avogadro constant (in mol^{-1}), k_B is the Boltzmann constant (in $kg\,m^2\,s^{-2}\,K^{-1}$), and T is the temperature (in K).

For a small length of a cell containing molecules pumped by a uniform power density P_p (in $W\,m^{-2}$) under steady-state condition:

$$\frac{dN_2}{dt} = R_p - N_2\Gamma = \frac{P_p\alpha_{02}}{h\nu_{02}} - N_2\Gamma = 0 \tag{9}$$

where R_p is the pumping rate (in $s^{-1}\,m^{-3}$), Γ is the relaxation rate (in s^{-1}), and α_{02} is the absorption coefficient of the pump transition (in m^{-1}). At low pressure, one can consider that relaxation is mainly due to collisions to the walls of the cell and that the effect of molecular collisions is negligible; Γ is then independent of the pair of transitions considered. α_{02} can be expressed as[48]

$$\alpha_{02} = S'_{02} g(\nu) N \tag{10}$$

where S'_{02} is the line strength (in $m^2\,s^{-1}$) and N is the total population in m^{-3}. S'_{02} contains all necessary information on level degeneracies, Einstein coefficient, and population (and is thus a function of the temperature).

Assuming the pump frequency is precisely tuned at the center of the pump transition and a Doppler profile, by combining the previous equations, Equation (8) becomes:

$$\gamma_0 = \frac{S'_{02} B_{21}}{\nu_{02}^2} \frac{Mc}{2\pi N_A k_B T} \frac{NP_p}{\Gamma} \tag{11}$$

The small-signal gain coefficient appears as the product of two factors:

$$\gamma_0 = G_m K \tag{12}$$

with

$$G_m = \frac{S'_{02} B_{21}}{\nu_{02}^2} \frac{Mc}{2\pi N_A k_B T} \tag{13}$$

and

$$K = \frac{NP_p}{\Gamma} \tag{14}$$

G_m in expressed in $m^4\,J^{-1}$ (uG_m), and K in $J\,m^{-5}$.

While the K factor depends on the experimental conditions and pump laser performances, the G_m factor depends almost exclusively (at the exception of the temperature) on spectroscopic parameters and on the choice of molecular gas. This molecular gain factor can thus be used as a figure of merit to classify the possible laser transitions of various gain media by their potential to lase.

4.3. Establishment of a Catalog of Ammonia THz Laser Transitions

Assuming the population inversion criterion is met for all pumped energy levels (and that the levels in the upper vibrational state are empty prior to pumping), one needs to possess several parameters in order to predict the list of possible THz laser frequencies using various IR pump transitions, and to calculate their molecular gain factors: 1) a list of vibrational transitions of the species (ν_{02} and involved quantum numbers); 2) their corresponding spectral line strengths (S'_{02}); 3) a list of pure rotational transitions within the lasing state (ν_{21} and involved quantum numbers); and 4) the Einstein coefficient B_{21} of these rotational transitions.

In the case of $^{14}NH_3$ and $^{15}NH_3$, all these parameters can conveniently be retrieved from the HITRAN online database[37] which was used to build the two catalogs in the present work. Listing all possible pairs of pump/laser lines by identifying all pump and laser transitions sharing the same upper state, is rather trivial; calculating the G_m values, however, require some care. Firstly, all entries in the HITRAN database are in CGS units. Secondly, the Einstein absorption coefficient A_{21} is reported for each transition and the corresponding B_{21} coefficient thus must be calculated. Thirdly, the S_{ij} ($S_{ij} = S'_{ij}/c \times 10^2$) values are reported at $T = 296$ K thus, for a laser operating at a significantly different temperature, the spectral line intensities have to be recalculated (see Ref. [48]). Here, all G_m calculations have been performed at $T = 296$ K. Finally, the S_{ij} values reported in HITRAN are weighted according to the natural terrestrial isotopic abundances I_a while in the present work the molecular gain factor is established for a given isotopologue (thus at 100 % abundance).

Expressed as a function of parameters directly extracted from HITRAN, Equation (13) becomes:

$$G_m = \frac{S_{02} A_{21}}{\tilde{\nu}_{02}^2 \tilde{\nu}_{21}^3} \frac{10^{-15} M}{16\pi^2 h I_a N_A k_B T} \tag{15}$$

$$\approx 3.88 \times 10^{12} \cdot \frac{S_{02} A_{21}}{\tilde{\nu}_{02}^2 \tilde{\nu}_{21}^3} \frac{M}{I_a} \tag{16}$$

with G_m in uG_m, S_{02} in $cm\,molecule^{-1}$ (HITRAN unit), A_{21} in s^{-1}, $\tilde{\nu}$ in cm^{-1}, M in $g\,mol^{-1}$, and I_a unitless ($I_a < 1$).

In our catalogs, we also report the polarization axis of the THz laser beam relative to the IR pump polarization. If $|\Delta J|_{02} = |\Delta J|_{21}$, the THz polarization axis is parallel to the IR pump one; otherwise it is perpendicular.[49] The frequencies of the THz laser transitions given in our tables correspond to the values given in HITRAN database. The corresponding uncertainty depends on the particular line and isotopologue, and typically ranges from 0.3 to 300 MHz for $^{14}NH_3$ and $^{15}NH_3$. Specific values can be retrieved from the HITRAN database.

4.4. Detection of Ammonia Laser Lines

A schematic representation of the optically pumped molecular laser set-up is given in **Figure 5**. This laser is an upgraded version of the one presented in Ref. [23]. One major evolution concerns the optical components (waveguide, input and output couplers) which are now placed under vacuum, in an 1.3 m-long cylindrical chamber. The cavity is composed of a 8 mm-internal diameter copper tubing terminated by flat input and output couplers, and the whole cylindrical chamber is filled with 10–30 µbar of a molecular gas acting as gain medium for the laser. This particular design, not as compact as the one presented in Ref. [26],
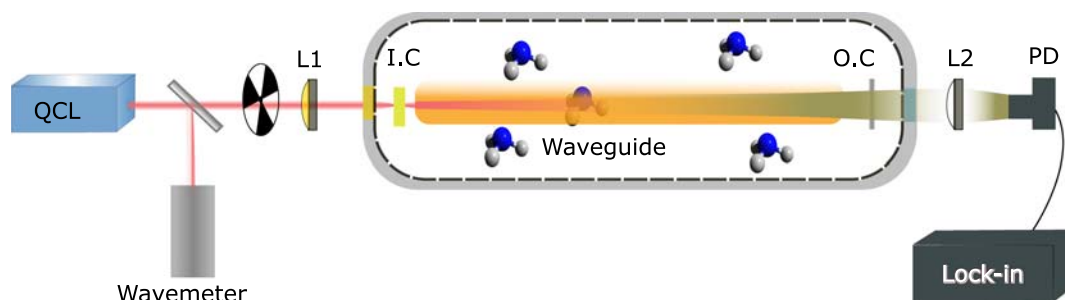
ADVANCED
SCIENCE NEWS
www.advancedsciencenews.com

ADVANCED
PHOTONICS
RESEARCH
Open Access
www.adpr-journal.com

Figure 5. Schematic of the molecular laser setup. Inside dashed line: under vacuum environment containing the gaseous gain medium at a pressure of a few tens of microbars. I.C: Input Coupler; O.C: Output Coupler; L1: ZnSe lens ; L2: Zeonex lens; PD: Pyroelectric Detector.

was optimized to enable THz lasing in a wide bandwidth, from 0.7 to about 5 THz. An external cavity QCL (MIRcat, DRS Daylight Solutions) operating between 920 and 1330 cm^{-1}, with a power of about 100 mW, is used for optical pumping of the molecular gas yielding population inversion. Here, the QCL allows to resonantly excite the rotational levels of the NH$_3$ ν_2 state. The QCL emitted frequency is measured by a wavemeter (Bristol Instruments 771B-MIR) with an accuracy of 1 ppm (i.e., 0.001 cm^{-1} at 1000 cm^{-1}). The QCL frequency is adjusted by modifying its temperature and/or its current. Some transitions are difficult to access due to mode hops in the external cavity QCL. The optics allowing the injection of the MIR radiation into the THz laser cavity consist of two gold-coated flat mirrors and a single ZnSe lens. The output window is made of TOPAS (cyclic olefin copolymer) and the THz laser radiation is collected and collimated using a Zeonex (cyclic olefin polymer) lens located outside the cylindrical chamber. Acting on the distance between input and output couplers allows us to tune the cavity in resonance with a THz transition, previously identified using our new catalogs. The emitted frequency is verified by scanning the cavity length of the molecular laser in order to measure the distance between successive Fabry–Perot modes, providing a rather good estimate of the laser wavelength.

The resulting THz laser power is measured using a pyroelectric detector (Sensor und Lasertechnik GmbH, THZ 10 HS, calibrated at PTB) by optically chopping the QCL radiation. Obviously the stability of the MIR radiation, both in terms of frequency and intensity, reflects directly on the power oscillations of our THz laser. While rapid oscillations were observed in our previous prototype, the new design presented in this work allows relatively long-term stability of the emitted power (weak fluctuations measured over 45 min). An example of power stability recording at 5.048 THz is shown in Figure S3, Supporting Information. Four typical spectra of THz laser emission for lines around 1 THz are shown in Figure S4, Supporting Information. The typical discrepancy between the measured peak frequency and the value given in the HITRAN database is less than 1 MHz. The typical linewidth is few 10s of kHz.

4.5. Measurement of the Gain Value and Estimation of the Relaxation Rate

Measurements of the small-signal gain γ_0 have been performed using an experimental setup described in detail in Mičica et al.[50]

The gain medium is enclosed at very low pressure (2 Pa) in a 46 cm-long/10 mm-internal diameter cell. It is optically seeded by a beam produced by a vector network analyzer (VNA) at the target THz frequency (750–1100 GHz). An amplification of the THz beam occurs, thanks to the gain medium pumped by a MIR QCL (having a parallel polarization to the THz beam), and can be measured using the second port of the VNA. The gain value is obtained by the ratio between the THz power measured with and without gain medium inside the gas cell. The pairs of corresponding pump/probe transitions are reported in Table S7, Supporting Information.

As previously described, γ_0 grows linearly with the molecular gain factor G_m. The relaxation rate Γ can be deduced from the slope $K = NP_p/\Gamma$ by fitting the curve of Figure 4. Chevalier et al.[25] have expressed the relaxation rate induced by collisions on the walls at very low pressure as $\Gamma = 2u/(3r)$, where $u = \sqrt{8k_B T/\pi m} = 607$ m s^{-1} is the average absolute molecular velocity calculated for ^{14}NH$_3$, $m = M/N_A$ is the molecular mass, and $r = 5$ mm is the gas cell radius. Thus, we obtain $\Gamma_{NH3-wall} = 0.8 \times 10^5$ s^{-1}.

Under our experimental conditions, the mean free path is estimated as $l = k_B T/(\sqrt{2}\pi d^2 P)$. For $T = 296$ K, $P = 2$ Pa, and considering the molecular diameter of NH$_3$ $d = 3.1$Å, $l = 4.8$ mm. This value is in the same order of magnitude as the cell radius r, so the molecule–molecule collisions cannot be neglected compared to collisions on the walls. One can estimate the molecule–molecule collision rate as $\Gamma_{NH_3-NH_3} = u'/l = 1.8 \times 10^5$ s^{-1}. To consider the collision between two identical molecules, we use the reduced mass $\mu = m/2$ rather than m to calculate the average relative speed $u' = \sqrt{8k_B T/\pi\mu}$ which leads to $u' = \sqrt{2}u$. Thus, the global relaxation rate can be estimated to $\Gamma_{NH_3-wall} + \Gamma_{NH_3-NH_3} = 2.6 \times 10^5$ s^{-1}, which is in agreement with the value extracted from the fit in Figure 4.

Supporting Information

Supporting Information is available from the Wiley Online Library or from the author.

Acknowledgements

Conflict of Interest

The authors declare no conflict of interest.

Data Availability Statements

The data that support the findings of this study are available in the Supporting Information of this article.

Keywords

[1] J. C. Pearson, B. J. Drouin, S. Yu, *IEEE J. Microwaves* **2021**, *1*, 43.
[2] J. Liu, F. Merkt, *Appl. Phys. Lett.* **2008**, *93*, 131105.
[3] F. Hindle, G. Mouret, S. Eliet, M. Guinet, A. Cuisset, R. Bocquet, T. Yasui, D. Rovera, *Appl. Phys. B* **2011**, *104*, 763.
[4] V. A. Andreeva, O. G. Kosareva, N. A. Panov, D. E. Shipilo, P. M. Solyankin, M. N. Esaulkov, P. González de Alaiza Martínez, A. P. Shkurinov, V. A. Makarov, L. Bergé, S. L. Chin, *Phys. Rev. Lett.* **2016**, *116*, 063902.
[5] R. Köhler, A. Tredicucci, F. Beltram, H. E. Beere, E. H. Linfield, A. G. Davies, D. A. Ritchie, R. C. Iotti, F. Rossi, *Nature* **2002**, *417*, 156.
[6] Y. Ren, J. N. Hovenier, R. Higgins, J. R. Gao, T. M. Klapwijk, S. C. Shi, B. Klein, T.-Y. Kao, Q. Hu, J. L. Reno, *Appl. Phys. Lett.* **2011**, *98*, 231109.
[7] H.-W. Hübers, R. Eichholz, S. G. Pavlov, H. Richter, *J. Infrared Millimeter Terahertz Waves* **2013**, *34*, 325.
[8] H.-W. Hubers, M. F. Kimmitt, N. Hiromoto, E. Brundermann, *IEEE Trans. Terahertz Sci. Technol.* **2011**, *1*, 321.
[9] J. V. Siles, K. B. Cooper, C. Lee, R. H. Lin, G. Chattopadhyay, I. Mehdi, *IEEE Trans. Terahertz Sci. Technol.* **2018**, *8*, 596.
[10] S. Yu, B. J. Drouin, J. C. Pearson, T. Amano, *J. Mol. Spectrosc.* **2018**, *350* 30.
[11] A. Crocker, H. A. Gebbie, M. F. Kimmitt, L. E. S. Mathias, *Nature* **1964**, *201*, 250.
[12] P. D. Coleman, *J. Opt. Soc. Am.* **1977**, *67*, 894.
[13] T. Y. Chang, T. J. Bridges, *Opt. Commun.* **1970**, *1*, 423.
[14] C. O. Weiss, M. Fourrier, C. Gastaud, M. Redon, *Optically Pumped Far-Infrared Ammonia Lasers*, Springer, New York **1984**, pp. 277–335.
[15] D. T. Hodges, T. S. Hartwick, *Appl. Phys. Lett.* **1973**, *23*, 252.
[16] R. Cohen, K. Busarow, K. Laughlin, G. Blake, M. Havenith, Y. Lee, R. Saykally, *J. Chem. Phys.* **1988**, *89*, 4494.
[17] P. Verhoeve, E. Zwart, M. Versluis, M. Drabbels, J. Termeulen, W. Meerts, A. Dymanus, D. McLay, *Rev. Sci. Instrum.* **1990**, *61*, 1612.
[18] D. Boucher, R. Bocquet, J. Burie, W. Chen, *J. de Phys. III* **1994**, *4*, 1467.
[19] F. Lewen, E. Michael, R. Gendriesch, J. Stutzki, G. Winnewisser, *J. Mol. Specrosc.* **1997**, *183*, 207.
[20] J. E. McCord, A. A. Ionin, S. P. Phipps, P. G. Crowell, A. I. Lampson, J. K. McIver, A. J. W. Brown, G. D. Hager, *IEEE J. Quant. Electron.* **2000**, *36*, 1041.
[21] B. Debord, F. Amrani, L. Vincetti, F. Gérôme, F. Benabid, *Fibers* **2019**, *7*, 16.
[22] J. Faist, F. Capasso, D. L. Sivco, C. Sirtori, A. L. Hutchinson, A. Y. Cho, *Science* **1994**, *264*, 5158.
[23] A. Pagies, G. Ducournau, J.-F. Lampin, *APL Photonics* **2016**, *1*, 031302.
[24] A. Zubairova, M. Wienold, H.-W. Hübers, in *44th Int. Conf. on Infrared, Millimeter, and Terahertz Waves (IRMMW-THz)*, IEEE, **2019**, pp. 1–2.
[25] P. Chevalier, A. Amirzhan, F. Wang, M. Piccardo, S. G. Johnson, F. Capasso, H. O. Everitt, *Science* **2019**, *366*, 856.
[26] J.-F. Lampin, A. Pagies, G. Santarelli, J. Hesler, W. Hansel, R. Holzwarth, S. Barbieri, *Opt. Express* **2020**, *28*, 2091.
[27] M. Wienold, A. Zubairova, H.-W. Hübers, *Opt. Express* **2020**, *28*, 23114.
[28] J.-F. Lampin, O. Pirali, Z. S. Buchanan, S. Eliet, M.-A. Martin-Drumel, J. Turut, P. Roy, F. Hindle, G. Mouret, *Opt. Lett.* **2019**, *44*, 4985.
[29] *Reviews of Infrared and Millimeter Waves (Vol. 2): Optically Pumped Far-Infrared Laser*, (Eds: K. J. Button, M. Inguscio, F. Strumia), Springer, New York **1984**.
[30] T. Y. Chang, T. J. Bridges, E. G. Burkhardt, *Appl. Phys. Lett.* **1970**, *17*, 357.
[31] E. J. Danielewicz, C. O. Weiss, *Optics Commun.* **1978**, *27*, 98.
[32] E. J. Danielewicz, C. O. Weiss, *IEEE J. Quant. Electron.* **1978**, *14*, 222.
[33] R. A. Wood, B. W. Davis, A. Vass, C. R. Pidgeon, *Opt. Lett.* **1980**, *5*, 153.
[34] G. D. Willenberg, *Opt. Lett.* **1981**, *6*, 372.
[35] E. M. Frank, C. O. Weiss, K. Siemsen, M. Grinda, G. D. Willenberg, *Opt. Lett.* **1982**, *7*, 96.
[36] J. P. Gordon, H. J. Zeiger, C. H. Townes, *Phys. Rev.* **1954**, *95*, 282.
[37] I. Gordon, L. Rothman, C. Hill, R. Kochanov, Y. Tan, P. Bernath, M. Birk, V. Boudon, A. Campargue, K. Chance, B. Drouin, J.-M. Flaud, R. Gamache, J. Hodges, D. Jacquemart, V. Perevalov, A. Perrin, K. Shine, M.-A. Smith, J. Tennyson, G. Toon, H. Tran, V. Tyuterev, A. Barbe, A. Császár, V. Devi, T. Furtenbacher, J. Harrison, J.-M. Hartmann, A. Jolly, et al., *J. Quantit. Spectrosc. Radiat. Transfer* **2017**, *203*, 3.
[38] L. R. Brown, D. B. Peterson, *J. Mol. Spectrosc.* **1994**, *168*, 593.
[39] P. Chen, J. Pearson, H. M. Pickett, S. Matsuura, G. A. Blake, *J. Mol. Spectrosc.* **2006**, *236*, 116.
[40] V. Nemtchinov, K. Sung, P. Varanasi, *J. Quant. Spectrosc. Radiat. Transfer* **2004**, *83*, 243.
[41] E. Canè, G. Di Lonardo, L. Fusina, F. Tamassia, A. , *J. Chem. Phys.* **2019**, *150*, 194301.
[42] H. Pickett, R. Poynter, E. Cohen, M. Delitsky, J. Pearson, H. Müller, *J. Quant. Spectrosc. Radiat. Transfer* **1998**, *60*, 883.
[43] R. Güsten, H. Wiesemeyer, K. M. Menten, U. U. Graf, K. Jacobs, B. Klein, O. Ricken, C. Risacher, J. Stutzki, *Nature* **2019**, *568* 357.
[44] W. S. Benedict, E. K. Plyler, *Can. J. Phys.* **1957**, *35*, 1235.
[45] S. Urban, D. Papousek, M. Bester, K. Yamada, G. Winnewisser, A. Guarnieri, *J. Mol. Spectrosc.* **1984**, *106*, 29.
[46] K. Sung, S. Yu, J. Pearson, O. Pirali, F. K. Tchana, L. Manceron, *J. Mol. Spectrosc.* **2016**, *327* 1.

[47] B. E. A. Saleh, M. C. Teich, *Fundamentals Of Photonics – Third Edition*, Wiley, Hoboken, NJ **2020**.

[48] P. F. Bernath, *J. Quant. Spectrosc. Radiat. Transfer* **2020**, *240*, 106687.

[49] S. Ganichev, W. Prettl, *Intense Terahertz Excitation Of Semiconductors*, Oxford Science Publication, Oxford, UK **2005**.

[50] M. Mičica, S. Eliet, M. Vanwolleghem, R. Motiyenko, A. Pienkina, L. Margulès, K. Postava, J. Pistora, J.-F. Lampin, *Opt. Express* **2018**, *26*, 21242.

[51] S. Urban, D. Papousek, S. Belov, A. Krupnov, M. Tretyakov, K. Yamada, G. Winnewisser, *J. Mol. Spectrosc.* **1983**, *101*, 16.